AGU PUBLICATIONS

Tectonics

RESEARCH ARTICLE
10.1002/2013TC003502

**Key Points:**
- Long-term tectonic subsidence modeled to infer fault geometry
- Geometry of the seismogenic Shanchiao Fault in Taiwan was first illuminated
- Preexisting thrust and rift faults participate in postcollisional extension

**Supporting Information:**
- Text S1
- Figure S1
- Table S1

**Correspondence to:**
C.-T. Chen,
ctchen@earth.sinica.edu.tw

**Citation:**
Chen, C.-T., J.-C. Lee, Y.-C. Chan, C.-Y. Lu, and L. S.-Y. Teng (2014), Elucidating the geometry of the active Shanchiao Fault in the Taipei metropolis, northern Taiwan, and the reactivation relationship with preexisting orogen structures, *Tectonics*, *33*, 2400–2418, doi:10.1002/2013TC003502.

Received 27 NOV 2013
Accepted 5 NOV 2014
Accepted article online 10 NOV 2014
Published online 11 DEC 2014

# Elucidating the geometry of the active Shanchiao Fault in the Taipei metropolis, northern Taiwan, and the reactivation relationship with preexisting orogen structures

**Chih-Tung Chen[1], Jian-Cheng Lee[1], Yu-Chang Chan[1], Chia-Yu Lu[2], and Louis Suh-Yui Teng[2]**

[1]Institute of Earth Sciences, Academia Sinica, Taipei, Taiwan, [2]Department of Geosciences, National Taiwan University, Taipei, Taiwan

**Abstract** The Shanchiao Fault is an active normal fault with documented paleoearthquakes in the Taipei metropolis, Taiwan. While posing direct seismic threat on the multimillion population, its crustal-scale fault plane configuration has not been constrained. This study presents the first attempt to resolve the fault plane dip changes of the Shanchiao Fault within the upper crust by forward modeling late Quaternary deformation. Tectonic subsidence over the last ~23 ka is estimated from vertical displacements of a rapidly formed alluvial fan horizon deformed into a dramatic rollover monocline. A 2-D profile across the Shanchiao Fault is chosen for elastic half-space dislocation modeling, and the results suggest that the fault is listric in the shallow crust with an abrupt change from subvertical ramp (85°–75°) to near-horizontal flat (10°–15°) at 3–4 km depth, consistent with an origin from the inversion of an orogen-related thrust detachment. Given the presence of rift-related fabrics in the underthrust Chinese Continental Margin basement beneath the Taiwanese orogenic wedge, listric ramp-flat-ramp models with a second deeper bend to 60° dip are also tested. Reasonable fits with the geological observations are produced when the lower ramp is located at greater than 8 km depth, which correlates with the hypocentral location of a moderate earthquake in 2004. Joint reactivation of preexisting thrust and rift faults by the Shanchiao Fault is therefore plausible with implications for seismic hazard in the Taipei area.

## 1. Introduction

The Taipei Basin, containing the Taipei metropolis in northern Taiwan with more than 8 million inhabitants, is geologically a half graben formed through the successive slips of the Shanchiao Fault during the late Quaternary (Figure 1). Although confirmed to be active in the Holocene [*C.-T. Chen et al.*, 2010] with several inferred paleoearthquake events [*Huang et al.*, 2007], the crustal geometry of the Shanchiao Fault remained uncertain since no outcrop has been identified, and direct imaging of the fault is prevented by the lack of both seismic profiling and clustering of (micro) seismicity [*Wang et al.*, 2006] (Figure 2a). The only inference on the Shanchiao Fault crustal configuration is its structural inversion relationship with a former thrust, the Hsinchuang Fault, deduced from regional geological synthesis [*Wu*, 1965; *Chiu*, 1968; *Teng et al.*, 2001]. A promising alternative to explore the subsurface fault geometry lies in analyzing fault-driven deformation. The late Quaternary deposits in the Taipei Basin are genetically the growth sediments of the Shanchiao Fault, and the horizons contained may serve as tectonic subsidence markers [*C.-T. Chen et al.*, 2010]. The derived crustal geometry of the Shanchiao Fault is crucial not only for societal applications such as seismic hazard and mitigation assessment but also for knowledge on tectonic reactivation of preexisting structural fabrics: the northern Taiwan crust contains a succession of fold-thrust structures resulting from the Taiwan Orogen, and possibly normal faults formed during earlier rifting of the Asian continental margin prior to arc-continent collision [e.g., *Lin et al.*, 2003].

Preexisting fabrics as weak planes or zones are favored locations for the development of subsequent structures during tectonic regime changes. In many thrust belts, reverse faults are known to reactivate former normal faults in positive tectonic inversion [e.g., *Schmid et al.*, 1996]. Conversely, postcollisional normal faulting is also significantly influenced by the earlier formed thrust faults [e.g., *Constenius*, 1996; *D'Agostino et al.*, 1998], though reactivation in this case may be complicated by the mechanical infeasibility of normal-sense slip on preexisting low-angle thrust fault surfaces [e.g., *Sibson*, 1985; *Faccenna et al.*, 1995; *Collettini and*


©2014. American Geophysical Union. All Rights Reserved.

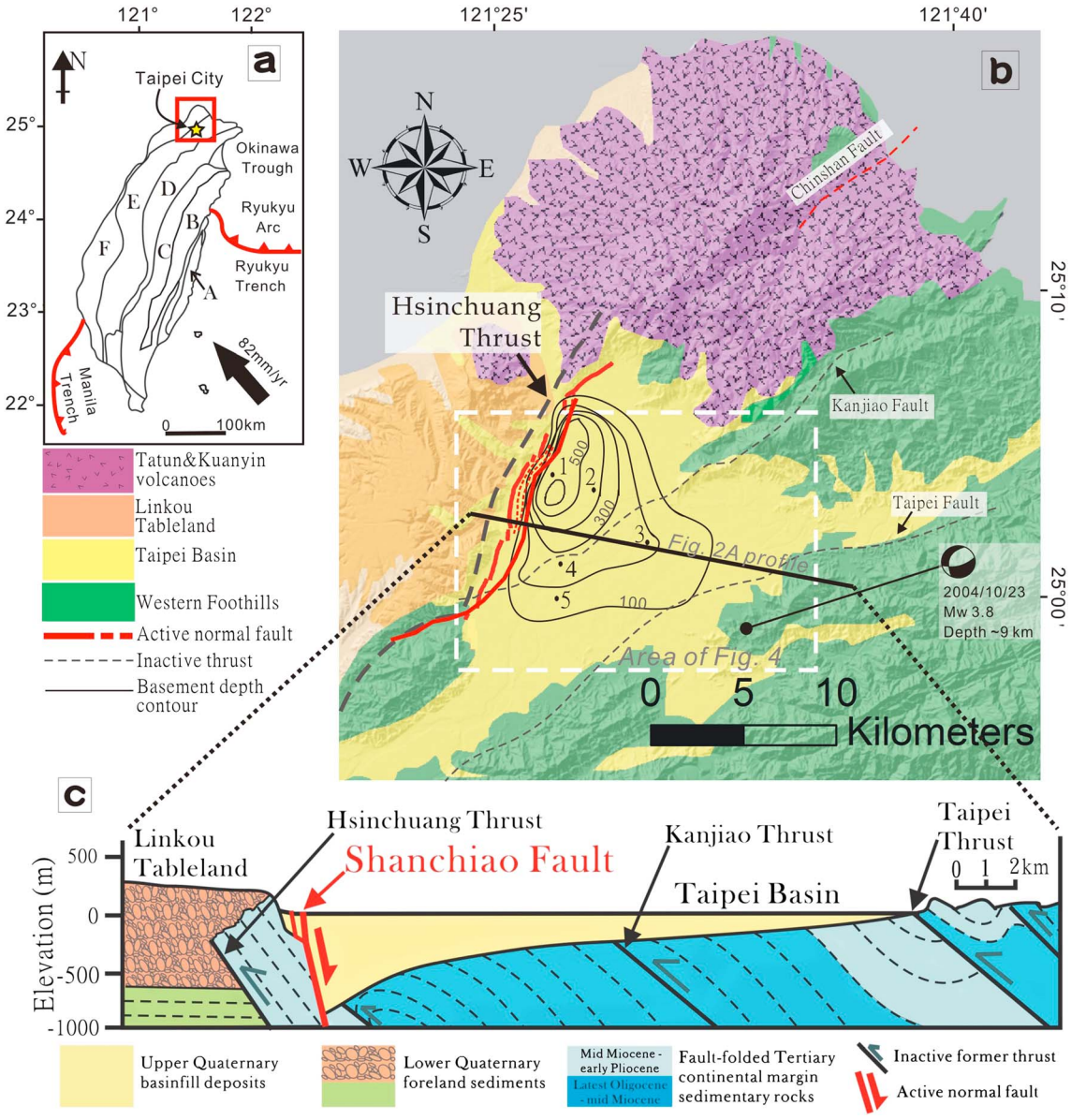


**Figure 1.** (a) General tectonic framework of Taiwan with major units indicated. A: accreted Luzon Arc sequence as orogen buttress; B: exhumed metamorphic Chinese Continental Margin basement; C: Backbone Range slate belt consisted of pelagic basement cover; D: Hsuehshan Range slate belt composed of margin graben infill; E: Foothills fold-thrust belt consisted of passive margin sequence; F: Coastal Plain underlain by Quaternary molasse sequence. (b) Simplified geology of the Taipei area. Thick red lines denote the Shanchiao Fault traces, and thin dashed grey lines mark inactive former thrusts. Thin black lines within the Taipei Basin are basement depth contours of 100 m interval (adapted from *Teng et al*. [2001]). Place names in the Taipei Basin mentioned in the text are marked by black dots: 1, Wuku; 2, Sanchung; 3, central Taipei; 4, Hsinchuang; and 5, Banchiao. Profile location of Figure 2a and areal extent of Figure 4 are indicated. Information and focal mechanism of a moderate (23 October 2004) earthquake related to the Shanchiao Fault (adapted from *Lee et al*. [2010]) is shown and referred in section 5. (c) Geological cross section of the Taipei Basin. The Hsinchuang, Kanjiao, and Taipei thrusts are inactive thrust faults which slipped during the collisional phase in the Taipei area.

*Sibson*, 2001; *Collettini*, 2011]. Previous analog modeling results show that former thrusts may be truncated (cut through) or partially to entirely reactivated by a newly formed normal fault depending on the dip of the thrust fault plane, with cutoff points around 32 and 41°, respectively [*Faccenna et al*., 1995]. Despite these arguments, development of new normal faults rooted into near-horizontal former thrust detachments is


©2014. American Geophysical Union. All Rights Reserved.

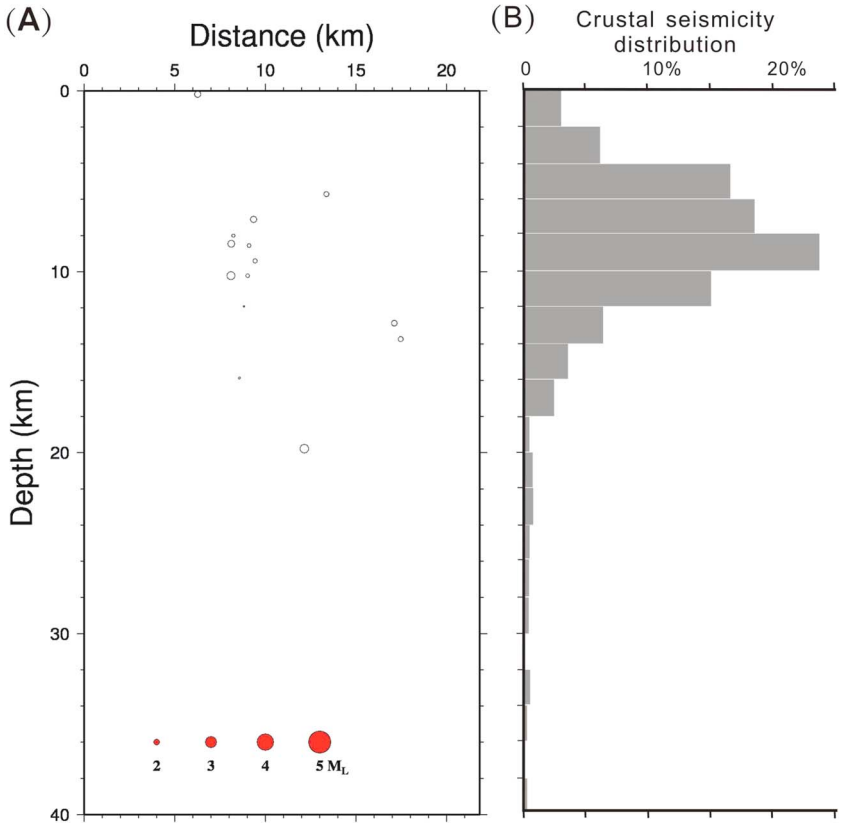


**Figure 2.** Seismicity of the studied region. (a) Earthquake distribution in a 4 km wide swath centered along profile line in Figure 1b from 1994 to 2013 (accessible from Geophysical Database Management System at Central Weather Bureau) [*Shin et al*., 2013], demonstrating the lack of both quantity and clustering of tectonic seismic events. (b) Depth distribution of crustal seismic events of the entire Taipei region, which is almost totally restricted within the top 20 km.

widely recognized and documented in the mid-Cenozoic collapse of the Cordilleran Orogen [e.g., *Constenius*, 1996]. For the late-Cenozoic destruction of the Apennines mountain chain, both reactivated thrusts and cross-cutting low-angle normal faults have been mapped and described [*D'Agostino et al*., 1998; *Tavarnelli et al*., 2003; *Collettini et al*., 2006]. Although former thrust planes of all ranges of dip have been observed to be reactivated as normal faults, the mechanical preconditions permitting such inversion, their seismogenic potential, and structural evolution remain much speculated [*Wernicke*, 1995; *Collettini*, 2011].

Less discussed is the possible role of preorogen normal faults in the postorogenic evolution of structures. Continental margins involved in collision belts often contain normal faults and rift structures [e.g., *Teng and Lin*, 2004; *Stampfli et al*., 2002; *Bonnet et al*., 2007]. These preexisting fabrics may influence the location and geometry of reverse faults during the incorporation and underthrusting of the continental margin basement. Though deeper in the orogenic pile when mountain building processes have reached climax, the preexisting normal faults may still have attitudes favorable for reactivation when they are under vertical $\sigma_1$ extensional environments.

The Taipei region in northern Taiwan presents a natural laboratory where a mature orogenic wedge fed by the rifted Chinese Continental Margin is experiencing extension/transtension during postorogenic collapse [*Teng*, 1996; *Hu et al*., 1996]. The sequence of thrust faults developed mainly within the margin and foreland sediments becomes inactive toward the north of the island as the compressive tectonic regime yields to the extensional one [*Lee and Wang*, 1988; *Hu et al*., 1996]. Furthermore, the underthrust Chinese Continental Margin contains normal faults, resulting from the opening of the South China Sea prior to the Taiwan Orogeny and mapped both in the foreland and beneath the fold-thrust belt [*Lin et al*., 2003; *Teng and Lin*, 2004; *Yang et al*., 2006]. The Shanchiao Fault, an active normal fault located in the northern tip of Taiwan Island, is thus a good candidate to explore how the late normal faults may reactivate former thrusts and possibly even


©2014. American Geophysical Union. All Rights Reserved.

previously formed normal faults. Given the clustering of moderate to large earthquakes at flat-ramp junctions and branch points found in the extensional fault systems of the Apennines [e.g., *Boncio and Lavecchia*, 2000a], the geometrical characteristics of the Shanchiao Fault may have important implications for its seismic hazard assessment as the Taipei metropolis is situated in the hanging wall vicinity of the fault.

As a first attempt to constrain the upper crustal geometry of the Shanchiao Fault, vertical displacement distribution across the Taipei Basin is documented from a key late Quaternary horizon within the hanging wall to constrain dislocation modeling of fault geometry. In light of regional tectonics, the best fit fault plane geometry is found to be closely associated with the reactivation of preexisting structures, allowing us to better address the earthquake hazard of the Shanchiao Fault.

## 2. Regional Setting

### 2.1. The Taiwan Orogen and Postcollisional Tectonics in Northern Taiwan

Taiwan is a product of active convergence between the Chinese Continental Margin and the Luzon Arc since around 5 Ma [*Ho*, 1986; *Suppe*, 1981; *Teng*, 1990; *Lu and Hsu*, 1992; *Wu et al*., 1997] with a rapid convergence rate of about 82 mm/yr currently in the NW direction [*Seno*, 1977; *Yu et al*., 1997] (Figure 1a). Prior to this Neogene orogeny, the Chinese Continental Margin south and east off the present Chinese coast was rifted due to the opening of the South China Sea [*Briais et al*., 1993; *Lee and Lawver*, 1994; *Lo et al*., 2000], leaving numerous rift-related normal faults and (half-) grabens whose magnitude of extension and subsidence increased eastward [*Lin et al*., 2003; *Teng and Lin*, 2004]. In the present day, the deformed and metamorphosed Chinese Continental Margin basement crops out along the eastern part of the Central Range against the accreted Luzon Arc of the Coastal Range (units A and B in Figure 1a). To the west, sediments on the rifted continental margin (units C–E) were deformed forming the slate belt and the Foothills fold-thrust belt with a sequence of west-vergent thrust faults which may root into detachments [e.g., *Suppe*, 1980; *Yue et al*., 2005; *Chen et al*., 2011]. These thrusts may have partially reactivated the rift-related normal faults [e.g., *Yang et al*., 2006; *Mouthereau and Lacombe*, 2006].

The oblique nature of the convergence between the continental margin and the arc leads to the southward propagation of the Taiwan Orogeny [*Suppe*, 1981; *Teng*, 1990]. Central and southern Taiwan are presently in full and mature collision [*Shyu et al*., 2005]; in contrast, the northern part of the mountain belt, including the Taipei metropolis region, is now in an extensional or transtensional tectonic setting [*Teng*, 1996; *Hu et al*., 2002] due to the westward advance of the Ryukyu subduction system and the postcollisional orogenic collapse [*Suppe*, 1984; *Teng*, 1996; *Wang et al*., 1999]. Active extension is evidenced by the presence of Quaternary extensional structures [*Lee and Wang*, 1988; *Lee*, 1989; *Lu et al*., 1995], extensional earthquake focal mechanisms [*Yeh et al*., 1991; *Kao et al*., 1998], and GPS displacement fields [*Yu et al*., 1997; *Rau et al*., 2008; *Lin et al*., 2010].

The Taipei Basin, where the Taipei metropolis resides, is a half graben formed in the hanging wall of the active Shanchiao normal fault. This fault is considered to be the major neotectonic structure responsible for the negative tectonic inversion (from contraction to extension) across the Taipei region [*Teng et al*., 2001] (Figure 1b), a process started at around 1 Ma contemporaneously with the vigorous eruptions of the Tatun volcanoes to the north of the Taipei Basin [*Wang and Chen*, 1990; *Song et al*., 2000]. The east-dipping Shanchiao Fault submerged the Foothills fold-thrust belt, composed of folded Oligo-Mio-Pliocene shallow marine sedimentary rocks, to constitute the basement of the Taipei Basin, and isolated a major mountain-front fan-delta [*Chen and Teng*, 1990] in the footwall to form the Linkou Tableland on the western border of the basin (Figure 1b). Submergence of the basin basement was recorded by the earliest basin deposits at ~0.4 Ma [*Wei et al*., 1998; *Teng et al*., 2001]. Since then the Taipei Basin has kept expanding due to erosion and tectonic subsidence by slips on the Shanchiao Fault, and an asymmetric wedge of unconsolidated fluvial, lacustrine, marine, and pyroclastic deposits has accumulated (Figure 3) that is thickest (more than 500 m) along the western margin of the basin (Figure 1).

### 2.2. The Active Shanchiao Fault

The surface trace of the Shanchiao Fault was mapped [*Chang et al*., 1998; *Lin et al*., 2000; *Lin*, 2001; *Huang et al*., 2007; *Chen*, 2012] close to the foothills of the Linkou Tableland (the Chinese translation of "Shanchiao Fault" is "Foothills Fault") and subparallel to the Hsinchuang Fault (Figure 1b) [*Lin*, 2001; *Teng et al*., 2001], with


©2014. American Geophysical Union. All Rights Reserved.

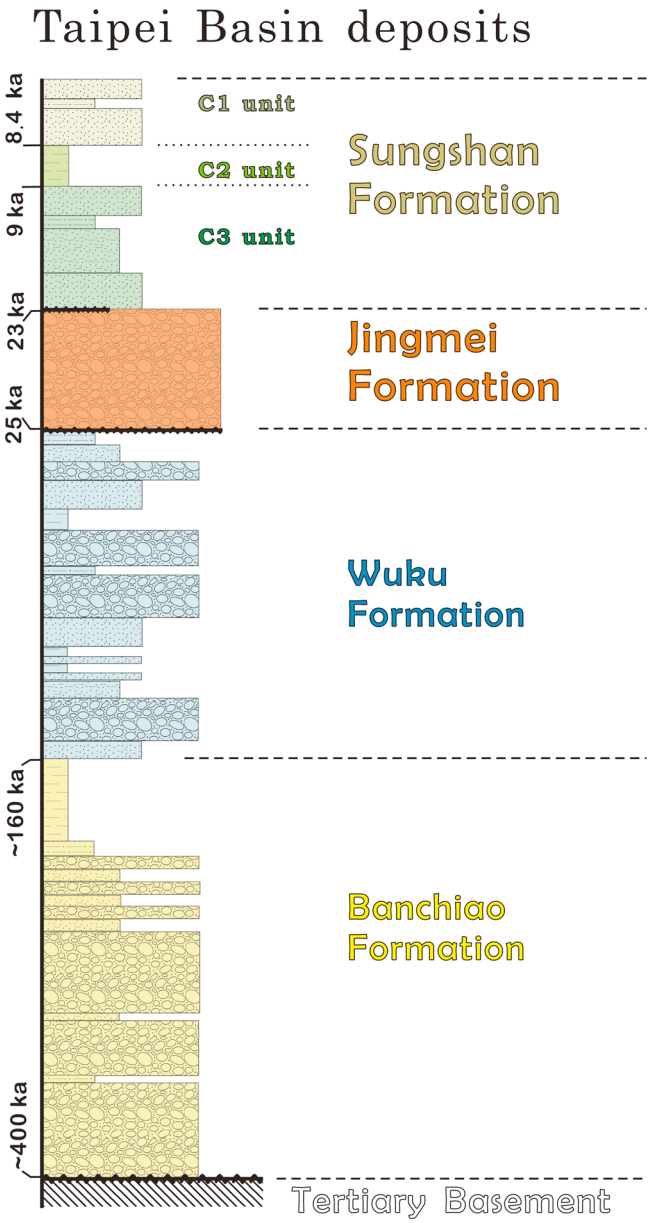


**Figure 3.** Lithostratigraphic column of the Taipei Basin deposits (after *Teng et al.* [1999]) reconstructed based on boreholes distributed throughout the basin. Not to scale.

features indicating that the steeper Shanchiao normal fault may merge into the Hsinchuang thrust fault at depth [*Wu*, 1965; *Chiu*, 1968]. Therefore, the Shanchiao Fault is interpreted to be inverted from the Hsinchuang Fault, the frontal thrust in northern Taiwan during the contraction phase [*Teng et al.*, 2001]. Left-lateral transcurrent motion associated with clockwise block rotation is also present together with downdip slips along the Shanchiao Fault, based on studies of regional structural geology, paleomagnetism, and GPS measurements [*Lu et al.*, 1995; *Lee et al.*, 1991; *Lee et al.*, 1999; *Rau et al.*, 2008].

Many efforts have been made to characterize this active fault. Shallow reflection seismic profiling across the Shanchiao Fault imaged vertical offsets of Holocene sediments, although the location of the main fault remains uncertain [*Hsieh et al.*, 1992; *Wang and Sun*, 1999; *Shih et al.*, 2004]. Preliminary geomorphic analysis [*Chen et al.*, 2006; *Chen*, 2012] also revealed a series of scarps closely related to the development of the Shanchiao Fault. GPS surveys of the Taipei area showed WNW-ESE extension with a slow rate of 0.08 μstrain/yr across the fault [*Yu et al.*, 1999]. Asymmetric tectonic subsidence related to the Shanchiao Fault was illuminated through 30 year long leveling data [*Chen et al.*, 2007] and recent interferometric synthetic aperture radar (InSAR) data [*Chang et al.*, 2010]. Holocene paleoseismic events were proposed at ~8500, ~9200, and ~11100 years B.P. from analysis of basin sediments retrieved from boreholes paired across branches of the fault [*Huang et al.*, 2007]. Radon and helium anomalies in soil-gas along the fault zone were documented, indicating the presence of a deep fracture-advection system [*Walia et al.*, 2005]. Growth faulting analyses at the central portion of the fault in Wuku and Luzhou areas [*C.-T. Chen et al.*, 2010; *Chen*, 2012] demonstrated that the fault has been constantly active in the last 23 kyr with averaged tectonic subsidence rates about 3 mm/yr; multiple fault planes were identified by the spatial partitioning of abovementioned tectonic subsidence across the fault, resembling a half-tulip structure within few hundred meters deep. The Shanchiao Fault is considered active [*Chang et al.*, 1998; *Lin et al.*, 2000] and seismogenic based on the Holocene paleoseismic events [*Huang et al.*, 2007] and a possible historic earthquake in 1694 suspected to induce severe subsidence and inundation in the Taipei Basin, forming the Kanghsi Taipei Lake [*Hsu*, 1983].


©2014. American Geophysical Union. All Rights Reserved.

Despite the knowledge gathered mostly about the current surface deformation and shallow underground properties of the fault, the geometry of the Shanchiao Fault at crustal scale has not been constrained. Efforts to delineate the fault plane shape at depth are hampered by the lack of deep seismic profiling data and the scarcity of upper crust microseismicity across northern Taiwan (Figure 2a) [*Wang et al*., 2006; *Wang*, 2008] (except in the Tatun Volcanoes north of the Taipei Basin where volcano-related seismic signals are identified) [*Lin et al*., 2005]. Another indirect way to elucidate the crustal fault geometry lies in analyzing hanging wall deformation which is intrinsically linked to the shape of the acting fault [e.g., *Gibbs*, 1983; *Suppe*, 1985; *Allmendinger and Shaw*, 2000]. In the case of the Shanchiao Fault, a key horizon widespread in the Taipei Basin, the Jingmei Formation top horizon, is identified from fault zone growth analyses [*C.-T. Chen et al*., 2010; *Chen*, 2012] as a tectonic subsidence marker encompassing vertical offsets accumulated over numerous earthquake cycles in the last 23 kyr. We first map the tectonic subsidence across the Taipei Basin by assembling the Jingmei Formation top horizon depths from borehole data and then model the displacement distribution with an elastic half-space boundary element method to fit fault geometry by a forward process. The favored fault geometries from the experiment results are discussed for their relations with preexisting tectonic structures including synconvergence thrusts and preorogen normal faults, and for the seismic hazard such fault configurations may imply.

## 3. Reconstruction of Late Quaternary Long-Term Accumulative Vertical Tectonic Deformation

### 3.1. The Jingmei Formation top Horizon as a Key Marker

Sedimentation in the Taipei Basin is controlled by tectonic subsidence and eustatic changes, due to its proximity in location and elevation to the sea [*Teng et al*., 2000]. During the height of the Last Glacial Maximum around 25 ka, the basin was under intense erosion due to the much lowered sea level (~140 m below the present-day level), exposing sediments well over 50 kyr old (the Wuku Formation) deposited in the previous interglacial period [*C.-T. Chen et al*., 2010]. As revealed in back stripping of growth sediments in the fault zone [*C.-T. Chen et al*., 2010; *Chen*, 2012], the basin ground composed of the Wuku Formation was around 70 m higher than the concurrent sea level at ~25 ka, resulting in strong denudation which prevented unambiguous preservation of fault scarps or offsets. While still in the height of the Last Glacial Maximum (LGM), rapid deposition of alluvial fan conglomerate that filled up incised valleys and then covered most of the ground in the Taipei Basin occurred between 25 and 23 ka in response to the capture of the Tahan River into the Taipei Basin, which previously flowed westward directly to the Taiwan Strait at Taoyuan southwest of Taipei [*Teng et al*., 2004; *Chen and Liu*, 1991]. This sedimentation event constitutes the Jingmei Formation as the bottommost member of the recent growth sediment sequence (Figure 3). The top of the Jingmei Formation, as the original alluvial fan surface, is expected to be a smooth, slightly conical plane at the time of deposition with the highest tip at the southwestern corner of the basin and sloping downward to north and northeast, as governed by the paleoflow of the Tahan River. Jingmei sedimentation ceased at 23 ka, before sea level began to rise, and was succeeded by deposition of fluvial to estuarine sand and mud designated as the Sungshan Formation, the topmost member of the basin deposits [*Teng et al*., 2000; *C.-T. Chen et al*., 2010] (Figure 3). However, the present configuration of the Jingmei Formation top horizon at the western edge of the Taipei Basin, as documented in channel-normal geological profiles in Wuku and Luzhou [*C.-T. Chen et al*., 2010; *Chen*, 2012], does not correspond to its initial fan surface level but exhibits drastic step-like downward offsets to the east within less than 1 km in the Shanchiao Fault zone as the product of normal faulting. The onlap and growth faulting features exhibited by the uppermost Sungshan Formation further confirm the tectonic nature of such horizon depth variations, and the conglomerate top horizon was found to faithfully record the vertical fault offsets following the completion of fan deposition at around 23 ka [*C.-T. Chen et al*., 2010; *Chen*, 2012].

The top of the Jingmei Formation, as the original Jingmei alluvial fan surface, therefore serves as a good marker documenting tectonic subsidence since about 23 ka. The Jingmei Formation top horizon is considered a key horizon with the following advantages: first, the Jingmei Formation was formed in a snapshot in geological sense and is widespread across the basin except the northwestern corner; also, the Jingmei Formation top horizon was expected to possess a regular, smooth, and slightly conical geometry originally as the top surface of a broad alluvial fan; furthermore, it is a distinct and easy-to-recognize lithological boundary in boreholes as the Jingmei Formation is the last conglomerate to be deposited


©2014. American Geophysical Union. All Rights Reserved.

(Figure 3) except in the northern corner (pyroclastic deposits sourced from the Tatun volcanoes) and the southeastern part (later fan deposits from the Xindian River) of the Taipei Basin. Besides, many boreholes drilled for engineering or construction purposes in the Taipei Basin encountered the conglomerate, making the depth information of this particular horizon widely available. Taking the possible earthquake recurrence interval as 1000 years from paleoseismic investigations by *Huang et al*. [2007], the Jingmei Formation top horizon has documented vertical fault displacement over at least ten earthquake cycles and is thus representative of late Quaternary long-term fault behavior.

### 3.2. Mapping of Tectonic Subsidence Across the Taipei Basin

In total, 520 borehole records with clear geological information in the Taipei Basin reaching the targeted Jingmei Formation top horizon are assembled in the data compilation (Figure 4; boreholes in the white dashed box area of Wuku-Sanchung-Taipei profile in Figure 4 are reported in Table S1 in the supporting information). In order to obtain true depth information, correction was made on every borehole by removing site elevation (0 as present sea level by Taiwan Datum; sixth column in Table S1) from the recorded depth value of the horizon (fourth column in Table S1); this "elevation-corrected horizon depth" (seventh column in Table S1) is referred simply as "horizon depth" in the following text. Before proceeding to evaluate the tectonic displacement, factors other than tectonics affecting the horizon depth distribution should be discussed. The greater horizon depths found near and north of the lower reach of the Tanshui River are probably a manifestation of the edge of the Jingmei alluvial fan, with possible contributions from Tanshui River channel erosion. Another lesser depression in the northeast boundary of the basin near the Keelung River channel is likely the eastern extension of the original fan periphery. The conical hump in the southeast is the subfan drained by the Xindian River, which was formed together with the main fan produced by the Tahan River and continued to be active beyond 23 ka till more recently [*Teng et al*., 2004]. The factors identified above are relatively local effects, and the first-order control on the marker horizon's elevation is still exerted by the slips of the Shanchiao Fault, especially concerning the channel-normal E-W (or more precisely, WNW-ENE) changes in fan conglomerate top surface elevation at the midfan to outer-fan portions in central Taipei. Channel-normal elevation variations between the axis and sides in middle to outer portions of modern alluvial fans in Taiwan [e.g., *Saito and Oguchi*, 2005] are typically very low as below 0.004, being at least one order less than the gradients of channel-parallel topography (generally between 0.04 and 0.004) [*Saito and Oguchi*, 2005]. The apparent downstream gradients of the Jingmei Formation top horizon are about 0.02–0.04 as deduced from depth differences of a few tens of meters from fan apex in southwestern basin corner to the inferred fan periphery near the lower reach of the Tanshui River (Figure 4), implying the channel-normal gradients are likely around 0.003 as equivalent to a few meters from fan axis to sides. Such variations inherited from original channel-normal fan topographic gradients are about 10% or less of maximum tectonic subsidence observed and are thus not considered to inflict significant bias in our tectonic subsidence estimates.

To extract the tectonic subsidence values of each well record, the horizon depth at SCF-1 in Wuku area (Figure 4) is taken as reference since the borehole is confirmed to be situated on the footwall and there is a near absence of both tectonic subsidence and uplift at this site. Such elevation stability at the SCF-1 site is inferred from fault zone growth analyses of the successive Sungshan Formation in which horizons are still at elevations corresponding to the sea level when they were formed [*C.-T. Chen et al*., 2010]. The resultant deduced cumulative tectonic subsidence distribution since ~23 ka is marked by contour lines in Figure 4. For the central section of the Taipei Basin, the hanging wall closest to the main fault experienced more than 70 m of vertical offset since the LGM, which rapidly decreases to about 30 m at a distance of 4 km away from the fault followed by a slower decline to about 10 m in the eastern margin of the basin 12 km away, resulting in a rollover monocline (Figure 5). Along-strike changes in the apparent tectonic offset are also significant, showing a somewhat steady southward decline from the center of the fault in Luzhou-Wuku area at more than 60 m to 30–40 m in Hsinchuang and about 10 m in Banchiao in the southern portion of the Shanchiao Fault. Based on the data and the rationale, fault-caused tectonic subsidence may persist further away from the fault into the Foothills east and south of the basin, as the depth of the Jingmei Formation top horizon near the eastern and southern basin borders is still greater than that of the SCF-1 on the fault footwall. It is also clear that the Shanchiao Fault is the major active fault within the Taipei Basin causing deformation since deposition of the Jingmei Formation, in agreement with previous geologic, geodetic, and geomorphic analyses


©2014. American Geophysical Union. All Rights Reserved.

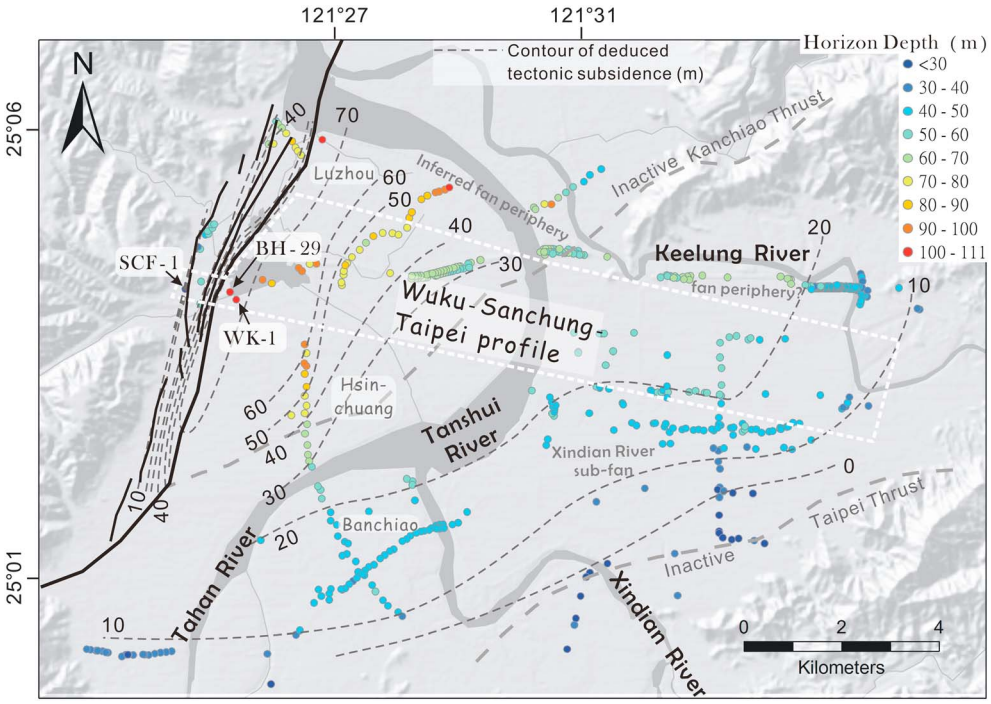


**Figure 4.** Basin-wide compilation of depth distribution of the Jingmei Formation top horizon from 520 borehole records (corrected depth). Boreholes are marked and color coded by horizon depth. Contour lines of post-LGM tectonic subsidence deduced from horizon depths (taking the value of SCF-1 as the footwall reference) are marked with 10 m interval. Boreholes included in the Wuku-Sanchung-Taipei profile are bracketed in the white dashed box. Inactive former thrusts are delineated with grey dashed lines, while the active Shanchiao Fault is marked in black (fault zone mapping from *Chen* [2012]). Place names and interpreted secondary features on the horizon depth distribution mentioned in the text are also denoted.

[*Teng et al.*, 2001; *Rau et al.*, 2008; *Chan et al.*, 2005; *Chen*, 2012]. The fault-parallel changes in the inferred vertical fault deformation may primarily reflect the diminishing displacement toward the southern fault tip, but contribution from the original fan topography, which should be higher upstream in the south with unresolved gradient, is of unknown proportion and difficult to evaluate and exclude.

Based on the above analysis, the WNW-oriented Wuku-Sanchung-Taipei profile (Figure 5) at the central part of both the fault and the Taipei Basin (Figure 4) is selected in order to best describe the tectonic subsidence imposed by the Shanchiao Fault on the Jingmei Formation top horizon. Its fault normal and paleoflow-normal orientation prevent inheriting major along-strike displacement variations and fan topographic gradients. Local factors concerning additional sediment sources as discussed previously are not apparently affecting the profile. Distribution of horizon depth in the Wuku-Sanchung-Taipei profile (Figure 5 and Table S1) is therefore most representative of the tectonic subsidence resulting from normal faulting with the variations governed principally by fault plane geometry and is chosen for investigating the geometrical characteristics of the Shanchiao Fault.

## 4. Half-Space Elastic Dislocation Modeling

### 4.1. Method and Setup

The long-term vertical tectonic deformation imposed by the Shanchiao Fault on the Jingmei Formation top horizon in the Wuku-Sanchung-Taipei profile is modeled by a boundary element method (BEM) using the Poly3D software [*Thomas*, 1993]. This method has been applied extensively to illuminate fault geometry or loading conditions utilizing deformed geological horizons or markers [e.g., *Willsey et al.*, 2002; *Hilley et al.*, 2010]. The long-term fault-related geological structures are considered as the sum of successive earthquake deformations [*Stein et al.*, 1988], with the seismogenic crust as elastic [e.g., *Gupta and Scholz*, 1998; *Benedette et al.*, 2000]. The method provides a full mechanical analysis satisfying rock stress-strain constitutive relations


©2014. American Geophysical Union. All Rights Reserved.

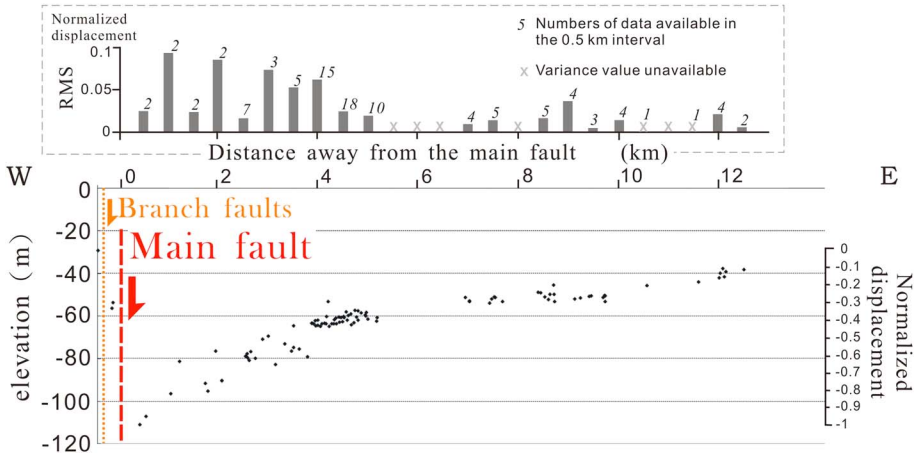


**Figure 5.** Variations of the Jingmei Formation top horizon depth taken as the geological constraint of post-LGM accumulative vertical tectonic deformation by the Shanchiao Fault in the Wuku-Sanchung-Taipei profile normal to the fault trace across the Shanchiao Fault, showing both the original depth values and normalized offset. Inset shows the scatter of the geological constraint as RMS values to the mean of each of the 0.5 km intervals.

to resolve how slip on a fault patch can produce displacements and stresses/strains within the half-space. The medium concerned is assumed to be isotropic and linear elastic with continuous stress and strain states except at the fault plane as a traction-free displacement discontinuity [*Okada*, 1985]. In the method, only the fault planes are discretized, avoiding errors from challenging meshing of the medium as required for finite element models. If both the fault geometry and slip distribution on the fault plane are known or determined, forward modeling yields the corresponding displacements. Finite element models may be able to generate more realistic results by including anisotropy and time/rate-dependent viscosity in the rheology [e.g., *Casey and Butler*, 2004]; however, the scarcity of relevant regional data does not help to reasonably constrain the additional involved parameters (especially knowledge on the loading history of the structures). Alternatively, kinematic reconstructions (inferring subsurface fault geometry from deformed geologic markers assuming volume conservation) [e.g., *Gibbs*, 1983; *Allmendinger and Shaw*, 2000] do not ensure stress equilibrium and are difficult to apply because the (near-) surface dip angle of the Shanchiao Fault is unknown. The BEM method, despite its restrictive assumptions, has been proven insightful in forward modeling of fault-deformed geological structures within the brittle upper crust [*Gupta and Scholz*, 1998; *Mynatt et al*., 2007; *Meigs et al*., 2008; *Hilley et al*., 2010] and is therefore employed for capturing the first-order geometric characteristics of the Shanchiao Fault. Should additional relevant data become available, rheologically more realistic modeling, which includes inelastic deformation and stress relaxation over geologic time, may be justified [e.g., *Stein et al*., 1988; *Armijo et al*., 1996].

In the case of the Shanchiao Fault, for which no exact information on its crustal geometry is available, numerous possible fault geometries whose dip varies with depth are tested against the offset pattern exhibited by the key horizon (Figure 5). Slip on the fault plane is assumed to be pure dip slip and uniform in magnitude along the entire fault plane due to lack of constraints. Variations in displacement magnitude with depth, if present, may affect chiefly detachment depth estimations [*Poblet and Bulnes*, 2005]. The parameters of crust elasticity applied in the forward modeling are adopted from those commonly used in previous works: the Young's modulus 7.5 GPa and Poisson's ratio 0.25 [e.g., *Cheng et al*., 2009]. The fault is restricted to extend to either 20 km depth, constrained from the exclusive depth distribution of regional crustal earthquakes ("seismogenic crust"; Figure 2b) as the probable thickness of elastic brittle crust in the Taipei area, or 30 km away from the fault trace, designated as twice the length of the observation from the Wuku-Sanchung-Taipei profile in order to prevent boundary effects in the region of interest (Figure 6). The strike direction (out of plane) width of the fault plane is 500 km, sufficiently long to avoid unintended 3-D boundary effects. The model results within 15 km from the fault are taken for evaluation and comparison with observation (records on footwall and within fault zone are excluded), and the readings are taken every 0.5 km in the horizontal direction. As the geological constraint from the key horizon contains only the vertical


©2014. American Geophysical Union. All Rights Reserved.

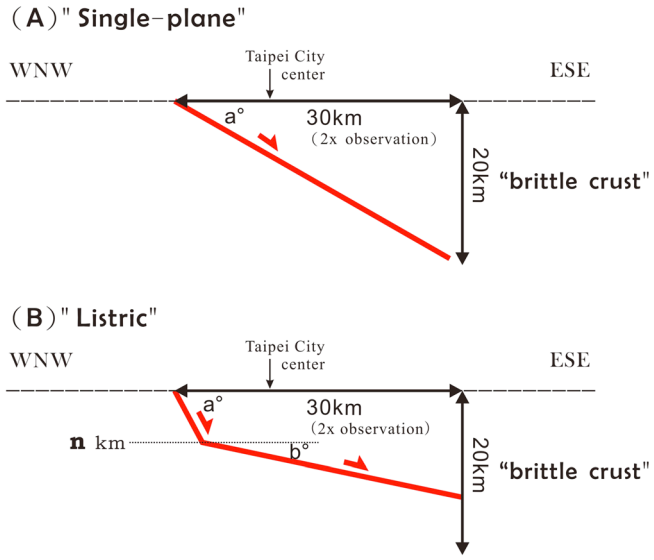


**Figure 6.** Geometric settings of the (a) uniform dip and (b) listric models in half-space elastic dislocation modeling. The single-plane model possesses only one parameter, the dip angle, "a." The listric model contains three variables: *a* for the dip angle of the upper portion, *b* for the dip angle of the lower portion, and *n* for the depth of the fault plane bend.

component of fault displacement, only the vertical component of the model displacement is taken into analysis. For realistic comparison between the geological record and model outcomes, both are parameterized by converting to ratios of offset at each point to that of the maximum offset. In the geological observation, the maximum vertical offset of about 80 m is found at borehole BH-29 near borehole WK-1 (the confirmed near-fault hanging wall location) [*C.-T. Chen et al.*, 2010], approximately 500 m away from the main fault trace. In the model results, the value 0.5 km away from the fault is thus taken as the maximum for each experiment. In order to quantitatively evaluate the model results and identify the ones that better reproduce the observed tectonic subsidence, the root-mean-square (RMS) of the vertical deviations between the geological record and model outcomes are calculated. In order to assess the quality of the data constraints, the scatter of the geological observation is also quantified for each of the 0.5 km intervals (Figure 5 inset; calculated as RMS of data from the mean of each of the 0.5 km intervals), which are generally low with slightly higher values within 4 km from the main fault trace.

### 4.2. Fault Plane Models With Uniform Dip

The first set of experiments assumes that the Shanchiao Fault has a constant dip within the elastic brittle crust. The dip angle, denoted as "a°" in Figure 6a, is tested with values of 45°, 60°, 75°, and 85°. The model results have large deviations from the geologic record as the RMS values are large (well over 0.3, Table 1), and they cannot reproduce the rapid decline in tectonic subsidence within 4 km from the fault trace (Figure 7). While all models overestimate the vertical offset, the higher-dip angle models of 75° and 85° yield results slightly closer to the observation with relatively lower RMS values, and do not possess an unrealistic concave-upward trend near the fault as seen in lower angle models (e.g., $a = 45°$; Figure 7). What can be inferred is that the Shanchiao Fault may be high angle in upper portions of its fault plane, but the uniform dip geometry with the inferred lower tip depth constraint does not fit the observed deformation pattern.

### 4.3. Fault Plane Models With Listric Geometry

From regional synthesis [e.g., *Teng et al.*, 2001] the Shanchiao Fault is considered a structural inversion of the Hsinchuang Thrust, suggesting that the Shanchiao Fault may possess a listric geometry by reslipping the former low-dipping thrust plane at depth. Here simplified listric geometry is reached by joining a shallow steep-dipping fault patch with a deeper gentle-dipping fault patch (Figure 6b), which contains three independent variables: the dip of the upper and lower fault patches ("a°" and "b°") and the depth of the junction point/line ("*n*" km). From the outcomes of the previous uniform dip experiments, the shallow patch is likely to be high angle (no less than 60°). The listric experiments are grouped in four according to the fault plane nodal point/line depth (*n*) shown in Table 1, and the complete results are presented in Figure S1 in the supporting information. For each nodal depth, experiments with "a" values of 75° and 60°, "b" values of 15°, 30°, and 45° were carried out. If the experiments produced results that closely resemble the geological observation, detailed dip variations were examined (e.g., "a" values of 85°, 80°, and 70°; "b" values of 5°, 10°, 20°, and 25°).


©2014. American Geophysical Union. All Rights Reserved.

**Table 1.** Summary of Deviations of Single-Plane and Listric Model Results to the Logarithmic Regression of the Geological Observation on Long-Term Tectonic Subsidence

| Geometry Style | Depth of Dip-Angle Change ("*n*" for Listric Models) | Dip-Angle Settings ("a" for Single Plane) ("a" and "b" for Listric) | Root-Mean-Square of Deviations From Natural Observation |
|---|---|---|---|
| Single plane | - | 85 | 0.305 |
| | | 75 | 0.326 |
| | | 60 | 0.377 |
| | | 45 | 0.454 |
| Listric | 2 | 75–45 | 0.202 |
| | | 75–30 | 0.135 |
| | | 75–15 | 0.084 |
| | | 60–45 | 0.280 |
| | | 60–30 | 0.172 |
| | | 60–15 | 0.073 |
| | 3 | 85–10 | 0.072 |
| | | 85–15 | 0.055 |
| | | 80–15 | 0.064 |
| | | 75–45 | 0.225 |
| | | 75–30 | 0.165 |
| | | 75–25 | 0.125 |
| | | 75–20 | 0.085 |
| | | 75–15 | 0.056 |
| | | 75–10 | 0.071 |
| | | 70–15 | 0.060 |
| | | 65–15 | 0.067 |
| | | 60–45 | 0.307 |
| | | 60–30 | 0.220 |
| | | 60–15 | 0.081 |
| | 4 | 85–15 | 0.083 |
| | | 85–10 | 0.059 |
| | | 85–5 | 0.076 |
| | | 80–15 | 0.088 |
| | | 80–10 | 0.063 |
| | | 75–45 | 0.253 |
| | | 75–30 | 0.206 |
| | | 75–15 | 0.097 |
| | | 75–10 | 0.070 |
| | | 75–5 | 0.077 |
| | | 60–45 | 0.334 |
| | | 60–30 | 0.274 |
| | | 60–15 | 0.154 |
| | 5 | 85–15 | 0.128 |
| | | 85–10 | 0.096 |
| | | 85–5 | 0.082 |
| | | 80–15 | 0.137 |
| | | 80–10 | 0.105 |
| | | 80–5 | 0.084 |
| | | 75–45 | 0.277 |
| | | 75–30 | 0.243 |
| | | 75–15 | 0.150 |
| | | 75–10 | 0.118 |
| | | 75–5 | 0.095 |
| | | 60–45 | 0.356 |
| | | 60–30 | 0.317 |
| | | 60–15 | 0.221 |

From the modeling outcomes, as shown in Figure 8 including selected results from experiment set of $n = 4$ km, the upper fault patch dip "a" was found to dominate the near-fault vertical displacement pattern, in which higher-displacement gradients are associated with steeper dips; meanwhile the lower patch dip "b" determines the far-field magnitude of tectonic subsidence, suggesting a correspondence between shallower dips and lesser subsidence amounts. Good fits (having the RMS values below 0.06) were obtained from


©2014. American Geophysical Union. All Rights Reserved.

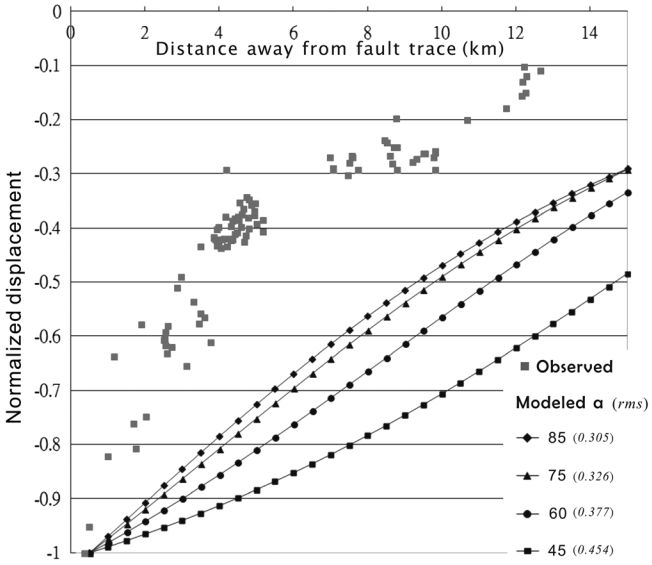


**Figure 7.** Modeling outcomes of the single-plane models. None of the models reproduced the observed rollover monocline; however, the higher-angle models ($a = 75°$ and 85°) are relatively closer to the geologic constraints. The RMS values as a measure of the vertical deviations between the model results and geological observations for all tested listric models are listed in Table 1.

experiments with a strong dip contrast between the upper and lower fault patches (Figure 9): in the case where the junction is 3 km deep, the upper patch dips quite steeply at 75–85° and the lower patch dips at 15°; for a 4 km node depth, the upper patch is dipping subvertically at 85° and the lower patch dips at 10°. It is notable that slight variations (5°) in the dip angle of the lower patch can bring about large variations to the output displacement pattern (Figures 8 and S1), and with increasing flat-ramp nodal depth (*n*) the change of displacement gradient from the near-fault to the far-field parts of the profile is smoother (Figures 9 and S1).

## 5. Discussions

### 5.1. Shallow Fault Geometry and its Relation With Synconvergence Thrust Detachment

The modeling results, albeit performed under rather simplified and idealistic conditions and geometrical settings, provide us with first-order control and insight on the geometry of the Shanchiao Fault at crustal scale. A drastic bend of the fault plane from near vertical to subhorizontal at 3 to 4 km depths is the main characteristic of the Shanchiao Fault in the shallow crust. The ramp part of the fault plane above the bend dips from 75° to almost vertical, and the flat part below the bend dips around 15°. The fault plane of all models producing good fit does not go deeper than 16 km within the modeled space. The subvertical dip at shallow depth and the dramatic curve toward subhorizontal are necessary to produce the pronounced rollover folding of the hanging wall and the rapid decline in tectonic subsidence away from the fault (Figure 9). The misfit of model output with the observed displacement pattern further away from the fault at about 6 to 13 km, though uncertainties in the geological record may exist, demonstrates the ambiguity of the fault plane dip at greater depths.

Inferences from regional geologic evidence on tectonic deformation agree with the modeling results on the listric nature of fault geometry. The listric character of the Shanchiao Fault is supported by the rollover monocline/reverse drag in the hanging wall (Figures 4 and 5) [*Wernicke and Burchfiel*, 1982], plus the near absence of uplift in the footwall (from fault zone growth analysis) [*C.-T. Chen et al.*, 2010] as a key property for inferring listric geometry in normal fault systems [*Resor and Pollard*, 2012].

The shallow dip of the lower fault portion illustrated above demonstrates a high possibility that the Shanchiao Fault results from negative tectonic inversion of a preexisting thrust fault plane. The best candidate for the reactivated structure is the Hsinchuang Fault, the former frontal thrust in northern Taiwan when the region was in its contraction phase [*Teng et al.*, 2001]. The Hsinchuang Fault outcrops along and slightly west of the topographic divide between the Linkou Tableland and the Taipei Basin (Figure 1), more than 1 km west of the Shanchiao Fault. The Hsinchuang Fault possesses a moderate-dipping ramp structure near ground surface and rapidly turned to be a gentle-dipping flat plane a few kilometers deep in southern Linkou Tableland [*Chiu*, 1968; *Suppe*, 1980]. The Hsinchuang Fault is therefore very low dipping (~15°) from around 3 km deep onward according to our results and may root into the master detachment of the western foothills at the frontal part of the Taiwan orogenic wedge [*Suppe*, 1980]. At depths of less than 3–4 km, normal faulting is not sustained on the preexisting gentle-dipping fault plane and instead branches upward to form a new subvertical fault plane. The newly formed subvertical upper fault patch extends to the land surface


©2014. American Geophysical Union. All Rights Reserved.

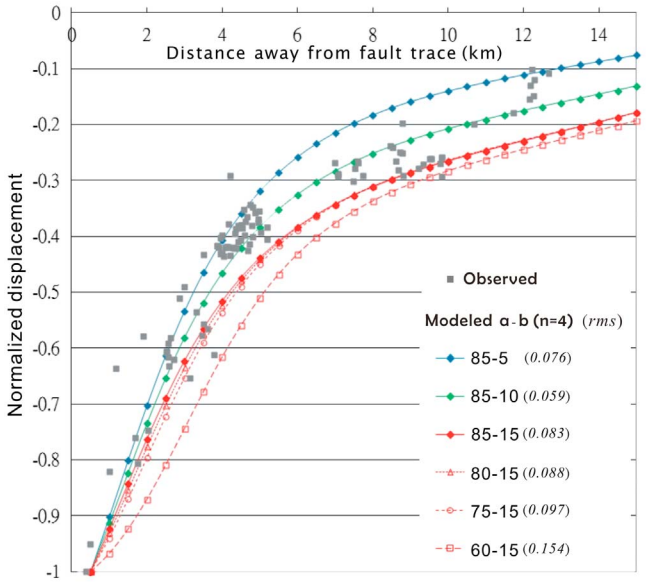


**Figure 8.** Selected modeling outcomes of the listric models with RMS values, demonstrating the effects of the varying ramp and flat dips (a and b values) on the offset pattern in the experiment set with nodal depth (value *n*) of 4 km. Please refer to the text for details. The RMS values as a measure of the vertical deviations between the model results and geological observations for all tested listric models are listed in Table 1.

producing the steep basin-basement gradient along the main fault in the Shanchiao Fault zone [*C.-T. Chen et al*., 2010; *Chen*, 2012] (Figure 1b).

In spite of rather good correlation to the regional preexisting thrust fault plane, normal faulting, especially substantial seismic slip, is thought difficult to be initiated or sustained with very gentle dipping configuration (e.g., 15° in the case of the Shanchiao Fault) in the brittle upper crust [*Anderson*, 1951; *Proffett*, 1977; *Sibson*, 1985, 2000]. Significant pore fluid overpressure and radical fault friction reduction by the massive presence of phyllosilicates, two mechanisms commonly cited for normal faults dipping less than 30° to be initiated or reactivated in a brittle extensional regime with vertical maximum principle stress [*Sibson*, 1985, 2000; *Axen*, 1992; *Collettini and Sibson*, 2001], are not observed in the upper crust and related thrust faults of northern Taiwan. The dips of the lower fault patch of the considered listric models and the Hsinchuang Fault itself are all below the lower bound value for partial reactivation of former thrust plane demonstrated in analog models by *Faccenna et al*. [1995]. In the following section further changes in fault plane geometry at depth are proposed and tested, exploring the plausible involvement of other preexisting structures, particularly the preorogen rift faults, for the Shanchiao Fault.

### 5.2. Possible Variations in Deeper Fault Geometry

#### 5.2.1. Half-Space Elastic Dislocation Modeling of Fault Plane Models With Double-Ramp Geometry

Based upon the above arguments, a set of experiments was designed to explore if an additional, steeper fault plane segment could be present below the low-angle portion of the Shanchiao Fault. The shallow part of the fault plane was modeled as listric as previously constrained, and a deeper steep fault patch is introduced, resulting in a ramp-flat-ramp geometry with two bends (Figure 10). Geometry of the shallow listric part is taken from one of the best fits (Figure 9) with parameters *a*, *b*, and *n* (Figure 6b) as 75°, 15°, and 3 km, respectively. The deeper fault patch as the second ramp is set to dip at 60°, the optimal angle for normal fault initiation and slip (assuming an Andersonian stress state and frictional coefficient of 0.6) which also corresponds well with the Oligo-Miocene synrift normal faults delineated in the seismic reflection profiles in western Taiwan [e.g., *Yang et al*., 2006]. The experiments are aimed at resolving the depth of the flat-ramp junction where the fault is bent downward between the intermediate and deep fault patches ("m" in Figure 10). The modeling outcome is presented in Figure 11 and Table 2. When the junction depth is shallower than 8 km, the double-ramp geometry produces an unrealistic anticline in the hanging wall instead of the rollover monocline revealed by the horizon depth distribution, and the model results in the anticline area significantly underestimate the vertical tectonic offset. When the junction depth is greater than 9 km, reasonable fits with the Jingmei Formation top horizon record are obtained, especially for $m = 12–13$ whose RMS values are equal to listric best fits. Compared with the listric best fits (Figure 9), the double-ramp models of $m = 9$ to 11 are able to envelope or contain the geologic data of the entire Wuku-Sanchung-Taipei profile.

Such ramp-flat-ramp geometry of normal faults, albeit not exclusive to the postorogenic tectonic environment, is recognized in several cases worldwide which possess hanging wall rollover folds similar to the Shanchiao Fault case [e.g., *Withjack and Schlische*, 2006]. Therefore, the double-ramp geometry with the


©2014. American Geophysical Union. All Rights Reserved.

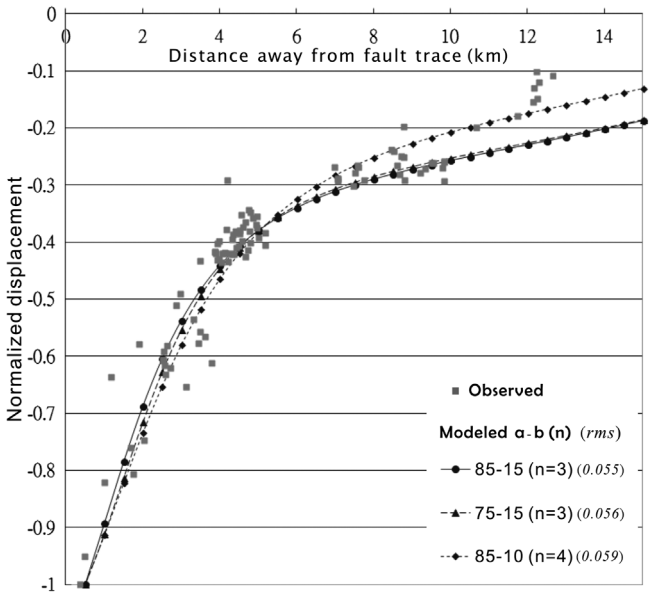


**Figure 9.** Modeling outcomes of the best fit experiments with RMS values. Please refer to the text for details. The RMS values as a measure of the vertical deviations between the model results and geological observations for all tested listric models are listed in Table 1.

deeper bend at more than 8 km depth is a plausible candidate along with the pure listric geometry for the crustal configuration of the Shanchiao Fault, as the present data control and modeling approach are insufficient in decisively discriminating the two rival geometries at more than around 8 km depths. Further geological and geodetic studies on tectonic subsidence beyond 15 km away from the fault might shed light on the deep structure of the Shanchiao Fault. Slip on the deep ramp may result in formation of an anticline (or a zone of lessened subsidence) and associated depositional characteristics (presence of diachronous unconformity and other changes in sediment layers depending on the aggradational or erosional nature of the environment) above the lower ramp in the double-ramp configuration [*Withjack and Schlische*, 2006]. None of these geologic phenomena are expected for a listric normal fault [*Withjack and Schlische*, 2006]. The flat-ramp junction of the Shanchiao Fault is projected slightly east of the basin periphery if the junction depth (m) is 9 km (and the deeper the junction the more eastward the position is projected); therefore, the features characteristic of the double-ramp geometry might be found in the Foothills east of the Taipei Basin. Possible verifications may come from contemporary vertical movement detected by leveling or InSAR, or stacking patterns of river/terrace deposition in the area.

### 5.2.2. The Role of Preorogen Rift Normal Faults on Postcollisional Extension Tectonics

The deeper steep fault patch in the double-ramp geometry illustrated above is a possible manifestation of the preorogen normal fault buried under the orogenic wedge. Rift normal faults are widespread on the Chinese Continental Margin [*Teng and Lin*, 2004], and one of them may be reactivated to constitute this deeper ramp instead of a newly formed structure. The rift normal faults were mainly active from Eocene to late Oligocene or earliest Miocene and extend from the thick continental margin sedimentary cover into the basement till probably midcrustal depth [*Teng*, 1992; *Lin et al*., 2003]. When incorporated into the collision zone, the preorogen normal faults are concealed mostly beneath the wedge as the main detachment in the Western Foothills fold-thrust belt is located within Miocene and latest Oligocene strata [*Suppe*, 1980], though their reverse faulting reactivation is also postulated [e.g., *Mouthereau and Lacombe*, 2006]. For northern Taiwan, the detachment level for the Hsinchuang Fault and regional décollement is considered to be in the bottom of the Wuchishan Formation deposited during the latest Oligocene, thus the rift-related normal faults contained within the lower continental margin sediments and the basement were underthrust below the frontal part of the orogenic wedge during the convergence. Although it is difficult to delineate from surface geological data,

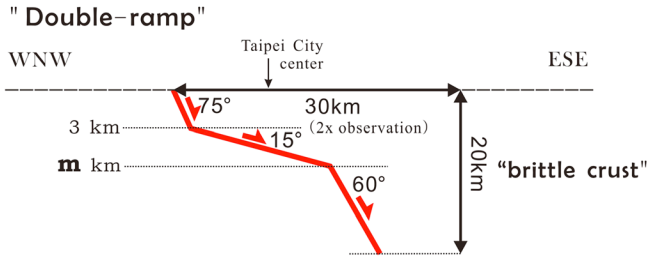


**Figure 10.** Geometrical setting of the double-ramp models in elastic half-space dislocation modeling. The listric part is adopted from one of the "best fit" models with the shallow ramp dipping at 75° which bends to 15° at 3 km depth. The tested variable is the depth "m" where the near-horizontal flat joins the deeper 60° ramp.


©2014. American Geophysical Union. All Rights Reserved.

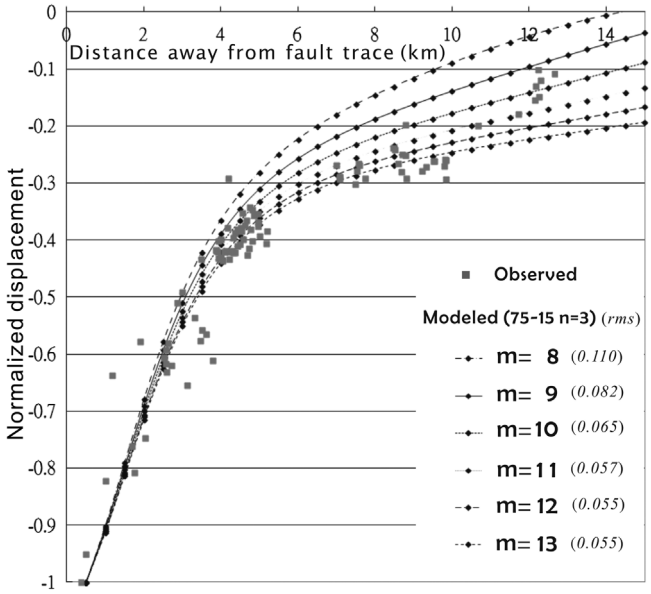


**Figure 11.** Selected modeling outcomes with RMS values of the double-ramp models with varying depth of the lower node from 8 to 13 km, demonstrating close fits with the geological tectonic subsidence record from the Jingmei Formation top horizon depth distribution. The RMS values as a measure of the vertical deviations between the model results and geological observations for all tested listric models are listed in Table 2.

geological structure analysis and seismic reflections in the vicinity indeed reveal a few pieces of evidence of the existence and tectonic inversion of these preorogen normal faults [e.g., *Yang et al*., 2006; *Mouthereau and Lacombe*, 2006]. The modeling results thereby suggest that, in northern Taiwan around the Taipei region, preorogen rift normal faults may be present under the fold-thrust pile, and the possibility that they are currently reactivated by the postorogenic extensional faulting should not be overlooked. To summarize, the double-ramp modeling results indicate that the Shanchiao Fault may have reactivated both the Hsinchuang Fault at intermediate depth (from ~3 to at least ~9 km) and a rift normal fault further deep (Figure 12).

Further possible supporting evidence for the deep steepening of the Shanchiao Fault plane comes from detailed relocation and focal mechanism determination of a $M_W$ 3.8 earthquake on 23 October 2004. The epicenter was located slightly east of the Taipei Basin eastern border at the toe of the Foothills (Figure 1), at depth estimated around 9 to 10 km [*Lin*, 2005; *K.-C. Chen et al*., 2010; *Lee et al*., 2010]. With improved inversion methods, the earthquake rupture source parameters from the determined focal mechanism point to a normal fault striking northeast and dipping about 60° to the southeast [*K.-C. Chen et al*., 2010; *Lee et al*., 2010]. The fault plane dip estimates and the focal center location are in agreement with the proposed double-ramp geometry whose lower bending nodal depth is more than 8 km deep, and the rupture was likely to have occurred on the upper boundary of the lower ramp fault patch (Figure 12). We therefore infer that the location where the reactivated thrust joined with the deeper rift normal fault, as the fault plane geometry made the second bend from near horizontal to ~60° dip, is at about 9 to 10 km deep. Another interpretation of this seismic event may be a minor rupture on a splayed branch fault within the Shanchiao Fault hanging wall, in line with the framework of *Abers* [2009]; in such case, the ruptured branch fault is either small in extent (consistent with the magnitude) or incipient in development as no known fault with post-LGM activity can be correlated with this branch fault.

### 5.3. Seismic Hazard Implication

Information on detailed fault plane geometry is essential in seismic hazard evaluation of active faults, as the width and hence area of the ruptured fault patch are proportional to the seismic moment, and the probable epicentral zones are dictated by fault configuration overlapping with seismogenic zone depths. Moderate to large earthquakes in extensional provinces are able to be generated at very shallow depths, up to 5 km deep, in areas like the northern Apennines [e.g., *Boncio et al*., 2004; *Chiaraluce et al*., 2005]. For the listric geometry best fit cases discussed previously, the seismogenic depths reside in the subhorizontal flat portion of the Shanchiao Fault which may generate low-angle normal faulting earthquakes like those documented by *Abers et al*. [1997]. The epicentral zone extends from the central part of the Taipei Basin, as the 5 km depth contour of the fault plane lies about 8 to 9 km away from the fault trace, to the eastern half of the Taipei Basin and much of the neighboring Foothills well into the Hsuehshan Range to the southeast, as the fault planes considered are still within the brittle crust (i.e., no deeper than 20 km) at the eastern end of the model space. For the double-ramp geometry proposed above, the possible seismogenic zone of


©2014. American Geophysical Union. All Rights Reserved.

**Table 2.** Summary of Deviations of Double-Ramp Model Results to the Logarithmic Regression of the Geological Observation on Long-Term Tectonic Subsidence

| Depth of the Lower Dip Angle Change (m) | Root-Mean-Square of Deviations From Natural Observation |
|---|---|
| 5 | 0.188 |
| 7 | 0.144 |
| 8 | 0.110 |
| 9 | 0.082 |
| 10 | 0.065 |
| 11 | 0.057 |
| 12 | 0.055 |
| 13 | 0.055 |

the Shanchiao Fault may also cover the eastern half of the Taipei Basin and only the northwestern part of the neighboring Foothills, as the fault planes concerned rapidly descend to over 20 km depth beyond the seismogenic crust in the lower ramp part of the designated configurations. Given the optimal attitude and its location within the seismogenic zone depths, the reactivated rift normal fault might be the initiation zone during seismic rupturing. In the mechanical framework of *Abers* [2009] the steep upper ramp of the fault, extending from land surface to 3–4 km depth, may also be seismogenic, thus forming a narrow epicentral strip about 1 km wide in the immediate hanging wall by the fault trace.

Another lesson from northern Apennines seismotectonics is the tendency of major earthquakes to cluster and nucleate at fault plane bends with prominent fault dip angle changes or the development of splaying branch faults, as revealed in the Narcia, Gubbio, and Colfiorito earthquake events [*Boncio and Lavecchia*, 2000a, 2000b]. Although the Shanchiao Fault lacks microseismicity along the fault plane as observed on the Altotiberina extensional detachment in the northern Apennines [*Chiaraluce et al.*, 2007], the shallow and deep ramp-flat junctions of the proposed listric and double-ramp fault plane geometries might be nucleation sites for important seismic events. This inference is also substantiated by the 23 October 2004 Taipei earthquake [*Lee et al.*, 2010; *K.-C. Chen et al.*, 2010] (Figure 1b) and two more successive seismic events ($M_L$ 3.2 and 3.7 on 23 March 2005 and 5 December 2005, respectively) [*K.-C. Chen et al.*, 2010] which all occurred in the same area and depth correlated to the shallow border of the lower fault ramp near the junction with the inverted thrust detachment. In map view, the shallow (listric bending about 3 to 4 km deep) and deep (about 9 km deep connection to rift normal fault) fault patch junctions are positioned around 1 and 15 km away from the fault trace.

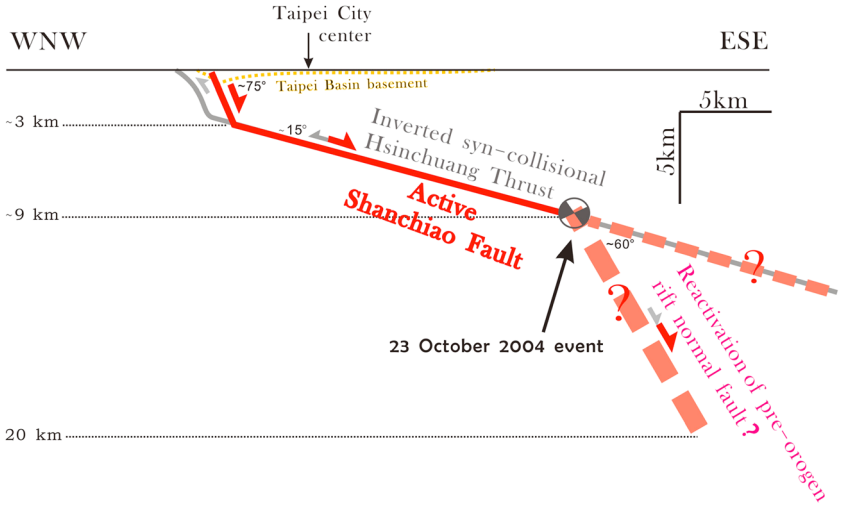


**Figure 12.** Interpretation of modeling results on the geometrical characteristics of the Shanchiao Fault in the seismogenic upper crust, illustrating the inversion of synconvergence Hsinchuang Thrust detachment and the possible reactivation of the preorogen rift normal fault.


©2014. American Geophysical Union. All Rights Reserved.

## 6. Concluding Remarks

With the aid of basin-wide geological record of long-term tectonic subsidence since the Last Glacial Maximum (~23 ka), the geometry of the Shanchiao Fault at crust scale is illuminated for the first time by half-space elastic dislocation modeling. The results suggest that the shallow portion of the fault plane is listric with a prominent change between 3 and 4 km deep from subvertical (85°–75°) to near-horizontal dips (~15°). For the deeper portion of the fault, another bending from subhorizontal to steep dipping (~60°) at more than 8 km depth is plausible. This model is consistent with the existence of preorogen normal fault underneath the fold-thrust pile and the few but well-resolved earthquake focal mechanisms. The Shanchiao Fault is therefore considered to possess a dramatic listric configuration by reactivating a synconvergence thrust detachment (the Hsinchuang Fault); at further depths, joint reslipping of a deeper preorogen rift normal fault beneath the detachment is possible, therefore resulting in double-ramp geometry. Both geometries place much of the Taipei metropolis region within the epicentral area of the Shanchiao Fault.

**Acknowledgments**

This research was supported by Institute of Earth Sciences, Academia Sinica, Department of Geosciences, National Taiwan University, and Ministry of Sciences and Technology, Taiwan, R.O.C. (grants NSC102-2116-M-001-016, NSC102-2116-M-001-002, NSC102-2116-M-002-022, MOST 103-2116-M-001 -005, and MOST103-2116-M-002 -018). We thank the technical support on seismic data from Wen-Tzong Liang, Kuan-Hsiang Chen, and the Taiwan Earthquake Research Data Center. We are grateful to Yue-Gau Chen and Jyr-Ching Hu at National Taiwan University, Jacques Malavieille at Geosciences Montpellier, and Ya-Ju Hsu and Shu-Hao Chang at Academia Sinica for their valuable support and stimulating discussions. Stephane Dominguez at Geosciences Montpellier is thanked for helpful comments on an earlier version of the manuscript. Constructive and detailed reviews from two anonymous reviewers, and positive comments and comprehensive English editing by Editors Nathan Niemi, Kirsten Cook, and John Geissman have greatly improved the manuscript and are deeply appreciated. This is a contribution of the Institute of Earth Sciences, Academia Sinica, IESAS1907.

## References

Abers, G. A. (2009), Slip on shallow-dipping normal faults, *Geology*, *37*, 767–768.

Abers, G. A., C. Z. Mutter, and J. Fang (1997), Shallow dips of normal faults during rapid extension: Earthquakes in the Woodlark-D'Entrecasteaux rift system, Papua New Guinea, *J. Geophys. Res.*, *102*, 15,301–15,317, doi:10.1029/97JB00787.

Allmendinger, R. W., and J. H. Shaw (2000), Estimation of fault propagation distance from fold shape: Implications for earthquake hazard assessment, *Geology*, *28*, 1099–1102.

Anderson, E. M. (1951), *The Dynamics of Faulting*, 2nd ed., 206 pp., Oliver and Boyd, Edinburgh.

Armijo, R., B. Meyer, G. C. P. King, A. Rigo, and D. Papanastassiou (1996), Quaternary evolution of the Corinth Rift and its implications for the Late Cenozoic evolution of the Aegean, *Geophys. J. Int.*, *126*, 11–53.

Axen, G. J. (1992), Pore pressure, stress increase, and fault weakening in low-angle normal faulting, *J. Geophys. Res.*, *97*(B6), 8979–8991, doi:10.1029/92JB00517.

Benedette, L., P. Tapponnier, G. C. P. King, B. Meyer, and I. Manighetti (2000), Growth folding and active thrusting in the Montello region, Veneto, northern Italy, *J. Geophys. Res.*, *105*(B1), 739–766, doi:10.1029/1999JB900222.

Boncio, P., and G. Lavecchia (2000a), A structural model for active extension in central Italy, *J. Geodyn.*, *29*, 233–244.

Boncio, P., and G. Lavecchia (2000b), A geological model for the Colfiorito earthquakes (September–October 1997, central Italy), *J. Seismolog.*, *4*, 345–356.

Boncio, P., G. Lavecchia, and B. Pace (2004), Defining a model of 3D seismogenic sources for Seismic Hazard Assessment applications: The case of central Apennines (Italy), *J. Seismolog.*, *8-3*, 407–425.

Bonnet, C., J. Malavieille, and J. Mosar (2007), Interactions between tectonics, erosion, and sedimentation during the recent evolution of the Alpine orogen: Analogue modeling insights, *Tectonics*, *26*, TC6016, doi:10.1029/2006TC002048.

Briais, A., P. Patriat, and P. Tapponnier (1993), Updated interpretation of magnetic anomalies and seafloor spreading stages in South China Sea: Implications for the tertiary tectonics of Southeast Asia, *J. Geophys. Res.*, *98*, 6299–6328, doi:10.1029/92JB02280.

Casey, M., and R. W. H. Butler (2004), Modelling approaches to understanding fold development: Implications for hydrocarbon reservoirs, *Mar. Pet. Geol.*, *21*, 933–946.

Chan, Y.-C., et al. (2005), Airborne laser swath mapping of the Metropolitan Taipei Area: Preliminary results and geological interpretations, *Workshop on Volcanic Activities and Sanchiao Fault in the Taipei Metropolitan Area* [in Chinese], pp. 87–102.

Chang, C.-P., J.-Y. Yen, A. Hooper, F.-M. Chou, Y.-A. Chen, C.-S. Hou, W.-C. Hung, and M.-S. Lin (2010), Monitoring of surface deformation in northern Taiwan using DInSAR and PSInSAR techniques, *Terr. Atmos. Ocean. Sci.*, *21-3*, 447–461.

Chang, H.-C., C.-W. Lin, M.-M. Chen, and S.-T. Lu (1998), An introduction to the active faults of Taiwan, explanatory text of the active fault map of Taiwan, *Special Publication of Central Geological Survey*, *10*, 1–103.

Chen, C.-T. (2012), Earthquake geology of the active Shanchiao Fault in the Taipei Metropolis, Taiwan, PhD dissertation, 195 pp., National Taiwan Univ., Taipei.

Chen, C.-T., J.-C. Lee, J.-C. Hu, Y.-C. Chan, and C.-Y. Lu (2006), The active Shanchiao Fault in the Metropolitan Taipei Area, Northern Taiwan: Geomorphic and geodetic analyses, *Eos Trans. AGU*, *87-52*, Fall Meeting Supplement, Abstract T33D–0543.

Chen, C.-T., J.-C. Hu, C.-Y. Lu, J.-C. Lee, and Y.-C. Chan (2007), Thirty-year land elevation change from subsidence to uplift following the termination of groundwater pumping and its geological implications in the Metropolitan Taipei Basin, Northern Taiwan, *Eng. Geol.*, *95*, 30–47.

Chen, C.-T., J.-C. Lee, Y.-C. Chan, and C.-Y. Lu (2010), Growth normal faulting at the western edge of the Metropolitan Taipei Basin since the Last Glacial Maximum, northern Taiwan, *Terr. Atmos. Ocean. Sci.*, *21*, 409–428.

Chen, C.-T., Y.-C. Chan, C.-Y. Lu, M. Simoes, and O. Beyssac (2011), Nappe structure revealed by thermal constraints in the Taiwan metamorphic belt, *Terra Nova*, *23*, 85–91.

Chen, K.-C., B.-S. Huang, W.-G. Huang, J.-H. Wang, K.-H. Kim, S.-J. Lee, Y.-C. Lai, S. Tsao, and C.-H. Chen (2010), A blind normal fault beneath the Taipei basin in northern Taiwan, *Terr. Atmos. Ocean. Sci.*, *21*, 495–502.

Chen, W.-F., and L. S. Teng (1990), Depositional environment of Quaternary deposits of the Linkou Tableland, northwestern Taiwan, *Proc. Geol. Soc. China*, *33*, 39–63.

Chen, Y.-G., and T.-K. Liu (1991), Radiocarbon dates of river terraces along the lower Tahanchi, north Taiwan: Their tectonic and geomorphic implications, *Proc. Geol. Soc. China*, *34*, 337–347.

Cheng, L. W., J.-C. Lee, J.-C. Hu, and H.-Y. Chen (2009), Coseismic and postseismic slip distribution of the 2003 $Mw = 6.5$ Chengkung earthquake in eastern Taiwan: Elastic modeling from inversion of GPS data, *Tectonophysics*, *466*, 335–343.

Chiaraluce, L., M. Barchi, C. Collettini, F. Mirabella, and S. Pucci (2005), Connecting seismically active normal faults with Quaternary geological structures in a complex extensional environment: The Colfiorito 1997 case history (northern Apennines, Italy), *Tectonics*, *24*, TC1002, doi:10.1029/2004TC001627.

Chiaraluce, L., C. Chiarabba, C. Collettini, D. Piccinini, and M. Cocco (2007), Architecture and mechanics of an active low-angle normal fault: Alto Tiberina Fault, northern Apennines, Italy, *J. Geophys. Res.*, *112*, B10310, doi:10.1029/2007JB005015.


©2014. American Geophysical Union. All Rights Reserved.

Chiu, H. T. (1968), The Hsinchuang Fault in the Taoyuan area, northern Taiwan, *Proc. Geol. Soc. China*, *11*, 60–73.
Collettini, C. (2011), The mechanical paradox of low-angle normal faults: Current understandings and open questions, *Tectonophysics*, *510*, 253–268.
Collettini, C., and R. H. Sibson (2001), Normal faults normal friction?, *Geology*, *29*, 927–930.
Collettini, C., N. De Paola, R. E. Holdsworth, and M. R. Barchi (2006), The development and behaviour of low-angle normal faults during Cenozoic asymmetric extension in the Northern Apennines, Italy, *J. Struct. Geol.*, *28*, 333–352.
Constenius, K. N. (1996), Late Paleogene extensional collapse of the Cordilleran foreland fold and thrust belt, *Geol. Soc. Am. Bull.*, *108*, 20–39.
D'Agostino, N., N. Chamot-Rooke, R. Funiciello, L. Jolivet, and F. Speranza (1998), The role of pre-existing thrust faults and topography of the styles of extension in the Gran Sasso range (central Italy), *Tectonophysics*, *292*, 229–254.
Faccenna, C., T. Nalpas, J.-P. Brun, and P. Davy (1995), The influence of pre-existing thrust faults on normal fault geometry in nature and in experiments, *J. Struct. Geol.*, *17*, 1139–1149.
Gibbs, A. D. (1983), Balanced cross-section construction from seismic sections in area of extensional tectonics, *J. Struct. Geol.*, *5*, 153–160.
Gupta, A., and C. H. Scholz (1998), Utility of elastic models in predicting fault displacement fields, *J. Geophys. Res.*, *103-B1*, 823–834, doi:10.1029/97JB03009.
Hilley, G. E., I. Mynatt, and D. D. Pollard (2010), Structural geometry of Raplee Ridge monocline and thrust fault imaged using inverse Boundary Element Modeling and ALSM data, *J. Struct. Geol.*, *32*, 45–58.
Ho, C.-S. (1986), A synthesis of the geological evolution of Taiwan, *Tectonophysics*, *125*, 1–16.
Hsieh, C.-H., Y.-F. Chang, and R.-H. Sun (1992), Seismic investigate Hsin-Chuan fault on the west of Taipei Basin, *Ti-Chih*, *12*, 13–26.
Hsu, M. T. (1983), Estimation of earthquake magnitude and seismic intensities of destructive earthquakes in the Ming and Ching eras, *Meteorol. Bull. Cent. Weather Bur.*, *29*, 1–18.
Hu, J.-C., J. Angelier, J.-C. Lee, H.-T. Chu, and D. Byrne (1996), Kinematics of convergence, deformation and stress distribution in the Taiwan collision area: 2-D finite-element numerical modeling, *Tectonophysics*, *255*, 243–268.
Hu, J.-C., S.-B. Yu, H.-T. Chu, and J. Angelier (2002), Transition tectonics of northern Taiwan induced by convergence and trench retreat, *Geol. Soc. Am. Spec. Pap.*, *358*, 149–162.
Huang, S.-Y., C. M. Rubin, Y.-G. Chen, and H.-C. Liu (2007), Prehistoric earthquakes along the Shanchiao Fault, Taipei Basin, northern Taiwan, *J. Asian Earth Sci.*, *31*, 265–276.
Kao, H., S. J. Shen, and K.-F. Ma (1998), Transition from oblique subduction to collision: Earthquakes in the southernmost Ryukyu arc-Taiwan region, *J. Geophys. Res.*, *103*, 7211–7229, doi:10.1029/97JB03510.
Lee, C.-T., and Y. Wang (1988), Quaternary stress changes in northern Taiwan and their tectonic implication, *Proc. Geol. Soc. China*, *31*, 154–168.
Lee, J.-C. (1989), Neotectonics of northern Taiwan based on the faults and paleostress analyses, MS thesis, 128 pp., National Taiwan Univ., Taipei.
Lee, J.-F., C.-Z. Lin, D.-C. Lai, T.-W. Su, Z.-L. Chiu, and C.-J. Zeng (1999), The study on the formation of Taipei Basin [in Chinese with English abstract], *Spec. Publ. Cent. Geol. Surv.*, *11*, 207–226.
Lee, S.-J., B.-S. Huang, W.-T. Liang, and K.-C. Chen (2010), Grid-based moment tensor inversion techniques by using 3-D Green's function database: A demonstration of the 23 October 2004 Taipei earthquake, *Terr. Atmos. Ocean. Sci.*, *21*, 503–514.
Lee, T.-Q., J. Angelier, H.-T. Chu, and F. Bergerat (1991), Rotations in the northeastern collision belt of Taiwan: Preliminary results from paleomagnetism, *Tectonophysics*, *199*, 109–120.
Lee, T.-Y., and L. A. Lawver (1994), Cenozoic plate reconstruction of the South China Sea region, *Tectonophysics*, *235*, 149–180.
Lin, A. T., A. B. Watts, and S. P. Hesselbo (2003), Cenozoic stratigraphy and subsidence history of the South China Sea margin in the Taiwan region, *Basin Res.*, *15*, 453–478.
Lin, C.-H. (2005), Seismicity increase after the construction of the world's tallest building: An active blind fault beneath the Taipei 101, *Geophys. Res. Lett.*, *32*, L22313, doi:10.1029/2005GL024223.
Lin, C.-H., K. I. Konstantinou, W.-T. Liang, H.-C. Pu, Y.-M. Lin, S.-H. You, and Y.-P. Huang (2005), Preliminary analysis of tectonic earthquakes and volcanoseismic signals recorded at the Tatun volcanic group, northern Taiwan, *Geophys. Res. Lett.*, *32*, L10313, doi:10.1029/2005GL022861.
Lin, C.-W., H.-C. Chang, S.-T. Lu, T.-S. Shih, and W.-J. Huang (2000), An introduction to the active faults of Taiwan, 2nd ed., explanatory text of the active fault map of Taiwan, *Spec. Publ. Cent. Geol. Surv.*, *13*, 1–122.
Lin, C.-Z. (2001), Geologic environment of the Taipei metropolis, paper presented at Symposium on Geological Hazards in the Taipei Metropolis, Taipei, Taiwan.
Lin, K.-C., J.-C. Hu, K.-E. Ching, J. Angelier, R.-J. Rau, S.-B. Yu, C.-H. Tsai, T.-C. Shin, and M.-H. Huang (2010), GPS crustal deformation, strain rate, and seismic activity after the 1999 Chi-Chi earthquake in Taiwan, *J. Geophys. Res.*, *115*, B07404, doi:10.1029/2009JB006417.
Lo, C.-H., S.-L. Chung, T.-Y. Lee, K.-L. Wang, and C.-T. Wu (2000), Cenozoic magmatism and rifted basin evolution around the Taiwan Strait, SE China continental margin, *Eos Trans. AGU*, *81*, 1111.
Lu, C.-Y., and K. J. Hsu (1992), Tectonic evolution of the Taiwan mountain belt, *Pet. Geol. Taiwan*, *27*, 21–46.
Lu, C.-Y., J. Angelier, H.-T. Chu, and J.-C. Lee (1995), Contractional, transcurrent, rotational and extensional tectonics: Examples from northern Taiwan, *Tectonophysics*, *246*, 129–146.
Meigs, A. J., M. L. Cooke, and S. T. Marshall (2008), Using vertical rock uplift patterns to constrain the three-dimensional fault configuration in the Los Angeles Basin, *Bull. Seismol. Soc. Am.*, *98*, 106–123.
Mouthereau, F., and O. Lacombe (2006), Inversion of Paleogene Chinese continental margin and thick-skinned deformation in the western foreland of Taiwan, *J. Struct. Geol.*, *28*, 1977–1993.
Mynatt, I., G. E. Hilley, and D. D. Pollard (2007), Inferring fault characteristics using fold geometry constrained by Airborne Laser Swath Mapping at Raplee Ridge, Utah, *Geophys. Res. Lett.*, *34*, L16315, doi:10.1029/2007GL030548.
Okada, Y. (1985), Surface deformation due to shear and tensile faults in a half-space, *Bull. Seismol. Soc. Am.*, *75*, 1135–1154.
Poblet, J., and M. Bulnes (2005), Fault-slip, bed-length and area variations in experimental rollover anticlines over listric normal faults: Influence in extension and depth to detachment estimations, *Tectonophysics*, *396*, 97–117.
Proffett, J. M. (1977), Cenozoic geology of the Yerington district, Nevada, and implications for the nature of Basin and Range faulting, *Geol. Soc. Am. Bull.*, *88*, 247–266.
Rau, R.-J., K.-E. Ching, J.-C. Hu, and J.-C. Lee (2008), Crustal deformation and block kinematics in transition from collision to subduction: Global positioning system measurements in northern Taiwan, 1995–2005, *J. Geophys. Res.*, *113*, B09404, doi:10.1029/2007JB005414.
Resor, P. G., and D. D. Pollard (2012), Reverse drag revisited: Why footwall deformation may be key to inferring listric fault geometry, *J. Struct. Geol.*, *41*, 98–109.
Saito, K., and T. Oguchi (2005), Slope of alluvial fans in humid regions of Japan, Taiwan, and the Philippines, *Geomorphology*, *70*, 147–162.


©2014. American Geophysical Union. All Rights Reserved.

Schmid, S. M., O. A. Pfiffner, N. Froitzheim, G. Schönborn, and E. Kissling (1996), Geophysical-geological transect and tectonic evolution of the Swiss-Italian Alps, *Tectonics*, *15*, 1036–1064, doi:10.1029/96TC00433.
Seno, T. (1977), The instantaneous rotation vector of the Philippine sea plate relative to the Eurasian plate, *Tectonophysics*, *42*, 209–226.
Shih, R.-C., Y.-H. Chan, and H.-C. Liu (2004), Shallow seismic reflection surveys of the Shanchiao Fault in the Guandu Plain, *Spec. Publ. Cent. Geol. Surv.*, *15*, 1–11.
Shin, T.-C., C.-H. Chang, H.-C. Pu, H.-W. Lin, and P.-L. Leu (2013), The geophysical database management system in Taiwan, *Terr. Atmos. Ocean. Sci.*, *24*, 11–18.
Shyu, J. B. H., K. Sieh, Y.-G. Chen, and C.-S. Liu (2005), Neotectonic architecture of Taiwan and its implications for future large earthquakes, *J. Geophys. Res.*, *110*, B08402, doi:10.1029/2004JB003251.
Sibson, R. H. (1985), A note on fault reactivation, *J. Struct. Geol.*, *7*, 751–754.
Sibson, R. H. (2000), Fluid involvement in normal faulting, *J. Geodyn.*, *29*, 469–499.
Song, S.-R., S.-J. Tsao, and H.-L. Lo (2000), Characteristics of the Tatun volcanic eruptions, north Taiwan: Implications for a cauldron formation and volcanic evolution, *J. Geol. Soc. China*, *43*, 361–378.
Stampfli, G. M., G. D. Borel, R. Marchant, and J. Mosar (2002), Western Alps geological constraints on western Tethyan reconstructions, *J. Virtual Explorer*, *7*, 75–104.
Stein, R. S., G. C. P. King, and J. B. Rundle (1988), The growth of geological structures by repeated earthquakes 2. Field examples of continental dip-slip faults, *J. Geophys. Res.*, *93*(B11), 13,319–13,331, doi:10.1029/JB093iB11p13319.
Suppe, J. (1980), A retrodeformable cross section of northern Taiwan, *Proc. Geol. Soc. China*, *23*, 46–55.
Suppe, J. (1981), Mechanics of mountain building and metamorphism in Taiwan, *Mem. Geol. Soc. China*, *4*, 67–89.
Suppe, J. (1984), Kinematics of arc-continent collision, flipping of subduction and back-arc spreading near Taiwan, *Mem. Geol. Soc. China*, *6*, 21–33.
Suppe, J. (1985), *Principles of Structural Geology*, Prentice Hall, Inc., Englewood Cliffs, N. J.
Tavarnelli, E., P. Renda, V. Pasqui, and M. Tramutoli (2003), The effects of post-orogenic extension on different scales: An example from the Apennine-Maghrebide fold-and-thrust belt, SW Sicily, *Terra Nova*, *15*, 1–7.
Teng, L. S. (1990), Late Cenozoic arc-continent collision in Taiwan, *Tectonophysics*, *183*, 57–76.
Teng, L. S. (1992), Geotectonic evolution of Tertiary continental margin basins of Taiwan, *Pet. Geol. Taiwan*, *27*, 1–19.
Teng, L. S. (1996), Extensional collapse of the northern Taiwan mountain belt, *Geology*, *24*, 949–952.
Teng, L. S., and A. T. Lin (2004), Cenozoic tectonics of the China continental margin: Insights from Taiwan, in *Aspects of the Tectonic Evolution of China*, edited by J. Malpas et al., *Geol. Soc. London Spec. Publ.*, *226*, 313–332.
Teng, L. S., P. B. Yuan, P.-Y. Chen, C.-H. Peng, T.-C. Lai, L.-Y. Fei, and H.-C. Liu (1999), Lithostratigraphy of Taipei Basin deposits, *Cent. Geol. Surv. Spec. Publ.*, *11*, 41–66.
Teng, L. S., P. B. Yuan, N.-T. Yu, and C.-H. Peng (2000), Sequence stratigraphy of the Taipei Basin deposits: A preliminary study, *J. Geol. Soc. China*, *43*, 497–520.
Teng, L. S., C.-T. Lee, C.-H. Peng, W.-F. Chen, and C.-J. Chu (2001), Origin and geological evolution of the Taipei Basin, Northern Taiwan, *West. Pac. Earth Sci.*, *1*, 115–142.
Teng, L. S., T.-K. Liu, Y.-G. Chen, P.-M. Liew, C.-T. Lee, H.-C. Liu, and C.-H. Peng (2004), Influence of Tahan River capture over the Taipei Basin, *Geogr. Res.*, *41*, 61–78.
Thomas, A. L. (1993), Ploy3D: A three-dimensional, polygonal element, displacement discontinuity boundary element computer program with application to fractures, faults and cavities in the Earth's crust, MS thesis, 97 pp., Stanford Univ., Stanford, Calif.
Walia, V., T.-C. Su, C.-C. Fu, and T. F. Yang (2005), Spatial variations of radon and helium concentrations in soil gas across the Shan-Chiao fault, Northern Taiwan, *Radiat. Meas.*, *40*, 513–516.
Wang, C.-Y., and C.-T. Sun (1999), Interpretation of seismic stratigraphy in the Taipei Basin, *Cent. Geol. Surv. Spec. Publ.*, *11*, 273–292.
Wang, J.-H. (2008), Urban seismology in the Taipei metropolitan area: Review and perspective, *Terr. Atmos. Ocean. Sci.*, *19*, 213–233.
Wang, J.-H., M.-W. Huang, and W.-G. Huang (2006), Aspects of $M \geq 4$ earthquakes in the Taipei metropolitan area, *West. Pac. Earth Sci.*, *6*, 169–190.
Wang, K.-L., S.-L. Chung, R. Shinjo, C.-H. Chen, T. F. Yang, and C.-H. Chen (1999), Post collisional magmatism around northern Taiwan and its relation with opening of the Okinawa Trough, *Tectonophysics*, *308*, 363–376.
Wang, W.-S., and C.-H. Chen (1990), The volcanology and fission track age dating of pyroclastic deposits in Tatun volcano group, northern Taiwan, *Acta Geol. Taiwan*, *28*, 1–40.
Wei, K., Y.-G. Chen, and T.-K. Liu (1998), Sedimentary history of the Taipei Basin with constraints from thermoluminescence dates, *J. Geol. Soc. China*, *41*, 109–125.
Wernicke, B. (1995), Low-angle normal faults and seismicity: A review, *J. Geophys. Res.*, *100*(B10), 20,159–20,174, doi:10.1029/95JB01911.
Wernicke, B., and B. C. Burchfiel (1982), Modes of extensional tectonics, *J. Struct. Geol.*, *4*, 105–115.
Willsey, S. P., P. J. Umhoefer, and G. E. Hilley (2002), Early evolution of an extensional monocline by a propagating normal fault: 3D analysis from combined field study and numerical modeling, *J. Struct. Geol.*, *24*, 651–669.
Withjack, M. O., and R. W. Schlische (2006), Geometric and experimental models of extensional fault-bend folds, in *Analogue and Numerical Modelling of Crustal-Scale Processes*, edited by S. J. H. Buiter and G. Schreurs, *Geol. Soc. London Spec. Publ.*, *253*, 285–305.
Wu, F. T., R.-J. Rau, and D. Z. Salzberg (1997), Taiwan orogeny: Thin-skinned or lithospheric collision?, *Tectonophysics*, *274*, 191–220.
Wu, F.-T. (1965), Subsurface geology of the Hsinchuang structure in the Taipei Basin, *Pet. Geol. Taiwan*, *4*, 271–282.
Yang, K.-M., S.-T. Huang, J.-C. Wu, H.-H. Ting, and W.-W. Mei (2006), Review and new insights on foreland tectonics in western Taiwan, *Int. Geol. Rev.*, *48*, 910–941.
Yeh, Y.-H., E. Barrier, C.-H. Lin, and J. Angelier (1991), Stress tensor analysis in the Taiwan area from focal mechanisms of earthquakes, *Tectonophysics*, *200*, 267–280.
Yu, S.-B., H.-Y. Chen, and L.-C. Kuo (1997), Velocity field of GPS stations in the Taiwan area, *Tectonophysics*, *274*, 41–59.
Yu, S.-B., H.-Y. Chen, L.-C. Kou, C.-S. Hou, and C.-F. Lee (1999), A study on the fault activities of the Taipei Basin, *Cent. Geol. Surv. Spec. Publ.*, *11*, 227–251.
Yue, L.-F., J. Suppe, and J.-H. Hong (2005), Structural geology of a classic thrust belt earthquake: The 1999 Chi-Chi earthquake Taiwan (*Mw* = 7.6), *J. Struct. Geol.*, *27*, 2058–2083.


©2014. American Geophysical Union. All Rights Reserved.